Modelling propagation of wildfires using cellular automata

Bárbara Mota[1]

[1]*Departamento de Física, Instituto Superior Técnico, Universidade de Lisboa, Lisboa, Portugal*

We applied probabilistic cellular automata (CA) to simulate fire propagation of four large wind-driven wildfires that occurred in October 2017: Pataias-Burinhosa, Quiaios, Sertã and Arganil. The baseline model is a simplified version of the Alexandridis CA model. We included a wind rule that produces boosts in fire spread along the wind direction and captures the spotting effect. The modified model revealed to be adequate to simulate wind-driven wildfires by yielding realistic propagation in the case of fires taking place in flat and homogeneous regions. Results of Sertã's wildfire were specially improved. We further show that Sertã's wildfire could have spread to Pedrogão Grande if that region had not been burned in previous June. CA fire spread models are found to be of use in managing fire suppression resources.

I. INTRODUCTION

For the past decades, we have observed an increasing trend of the number, size and severity of wildfires in Portugal [1]. 2017 is the year that registered the largest burned area and number of lost lives due to wildfires (115). It is noteworthy that, in that year, the fire season unusually extended from June to October, and that June and October were the months that registered the most severe fire events [2].

The area burned in October corresponds to more than 50% of the total burned in 2017. On October 15, around 500 ignitions were reported and the fire spread was enhanced by meteorological conditions. The wind was strong and humidity low due to the close passage of hurricane Ophelia; most of the country was facing a very severe drought. All these factors combined with biomass availability led to some of the largest fire events ever seen in the country [3].

Wildfires constitute an environmental problem and are harmful to economy and society. Southern Europe is a wildfire-prone region, and recent studies anticipate that, due to climate change, fire events will take place more frequently and with greater severity [4], [5]. It is thus of the utmost importance that we understand how fire behaves, what are the underlying mechanisms and which factors influence its occurrence the most. Modelling fire propagation can incorporate this knowledge to better describe how fire interacts with landscapes under certain weather conditions. Models of fire spread can also be used to assess fire risk over different areas and, therefore, they can help in developing land management strategies.

Modelling fire spread is a complex task. Wildfires cannot be merely described by the physical and chemical mechanisms taking place at microscopic scales. One must consider the influence of the terrain as well as the meteorological conditions. The existence of significant slopes can either slow down (negative slopes, fire propagating downhill) or enhance fire spread (positive slopes, fire propagating uphill). Vegetation cover also plays an important role, since some species are more wildfire-prone. Lastly, wind can strongly affect the speed and direction of fire propagation [6].

In particular, cellular automata (CA) models of fire spread have been employed to simulate fire propagation of wildfires in Southern Europe [7], [8], [9]. CA models can be easily manipulated to include different propagation rules, factors and can integrate information on the terrain and meteorology. Another advantage of such models is that these are not as computationally demanding as vector-based models [7], which makes them viable tools to assist in firefighting.

Our goal is to model, both in space and time, the fire spread of large fire events that occurred in October 2017, in Portugal.

II. CELLULAR AUTOMATA AND MODELS OF FIRE SPREAD

Cellular automata are mathematical models defined spatially by a regular grid whose cells have a well-defined shape, such as square or hexagon. The dynamics of such models is introduced by a set of simple local interaction rules. At every discrete time step, these rules update the cells' states and can yield global complexity. A cell is only allowed to interact with neighbouring cells [10].

There is a great number of CA fire spread models. Their dynamics can be either deterministic, such as the model of Karafyllidis and Thanailakis [11], or probabilistic like the model of Li and Magill [12]. Although most models are described for square CA, there are examples of different geometries, as is the case of the model of Trunfio *et al.* whose grid is made of hexagonal cells [13].

The effect of fire suppression on fire spread has also been addressed by some of these models. For instance, Alexandridis *et al.* [8] employed the Aerial Dropping Model [14] into a CA fire spread model to include the effect of usage of aircrafts in fire combat.

CA wildfire models can be applied to perform fire risk assessment on specific regions. Fire risk maps can thus be used to devise efficient land management strategies that can minimise the size and risk of wildfires. Avolio *et al.* [15], Russo *et al.* [16] and Ohgai *et al.* [17] are examples of works which employed CA fire spread models to map fire risk.

III. METHODS AND DATA

A. Alexandridis CA model of fire spread

The Alexandridis CA model of fire spread was here employed as the baseline model [7]. Variations of this model were previously applied to simulate other fire events in Southern Europe [8], [9]. In this section, we describe the

main features of the Alexandridis model developed to simulate the wildfire that took place in Stepses (Greece) in 1990.

This model makes use of a two-dimensional grid composed of square cells with size L to discretise the study area. We chose a grid with $L = 100$ m. The neighbourhood of each cell is made of its eight nearest neighbours, as shown in Fig. 1. Interactions between cells can only take place inside these neighbourhoods. There are thus eight possible directions of fire propagation. Cells in the Alexandridis model can be in either one of four possible states:

State 1 The cell is void of fuel content. It is assumed that it cannot be ignited at any future moment.

State 2 The cell contains fuel. It can be ignited.

State 3 The cell has been ignited. The fire in this cell can be propagated to some cell(s) in its neighbourhood.

State 4 The fire in the cell extinguishes. Permanent state.

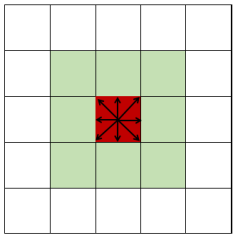

FIG. 1: Directions of fire spread in a two-dimensional cellular automata model. The cell in red is burning and all the cells in its neighbourhood (green cells) can be set on fire.

The state matrix contains the states of all cells at any moment of the simulation. The initial matrix is obtained using information on the land cover of the area under study. The influence of land cover, slope of the terrain wind speed and direction on fire propagation is included in p_{burn} which expresses the likelihood of fire spreading from a burning cell to a flammable cell, in its neighbourhood. It is defined by Eq. 1:

$$p_{burn} = p_h(1 + p_{veg})p_w p_s \tag{1}$$

where p_{veg}, p_w and p_s quantify the effect of the density of vegetation, the type of vegetation, the wind speed and direction and the slope of the terrain, respectively. The term p_h (optimised value: $p_h = 0.58$) represents the value of p_{burn} for a cell with certain vegetation characteristics and where the terrain is flat and no wind is felt. A time step Δt is defined beforehand and it remains fixed throughout the simulation. Between times t and $t + \Delta t$, the state matrix is updated according to a set of transition rules:

1. If state $(i, j) = 1$ at t, state $(i, j) = 1$ at $t + \Delta t$.
2. If state $(i, j) = 3$ at t, state $(i, j) = 4$ at $t + \Delta t$.
3. If state $(i, j) = 4$ at t, state $(i, j) = 4$ at $t + \Delta t$.
4. If state $(i, j) = 2$ at t, state $(i \pm 1, j \pm 1) = 3$ if the factor p_{burn} is higher than a value obtained by a random generator.

The rules here applied imply that: (i) a burning cell will be completely burned in the following time instant; (ii) once the fire is extinguished in a cell, it is impossible to ignite that cell at any future time of the simulation; (iii) fire propagates from a burning cell to a cell in its neighbourhood if the number p_{burn} computed for the latter is greater than a pseudo-random number. This last rule makes this model probabilistic.

Let us now see how the different factors in Eq. 1 are calculated. The wind factor p_w integrates two terms that account separately for the wind speed and direction (Eq. 2):

$$p_w = \exp\left(c_1 V\right) f_t \tag{2}$$

where c_1 is a constant, V is the wind speed and f_t is a function of the direction of the wind relative to the direction of fire propagation, θ: $f_t = \exp\left(V c_2(\cos\theta - 1)\right)$. Alexandridis *el al.* [7] obtained the values $c_1 = 0.045$ and $c_2 = 0.131$ by optimisation.

The slope factor term requires the inclination of the terrain to be locally determined, as shown in Eq. 3, where H_1 and H_2 are the elevation values for the neighbouring and burning cells, respectively, and $d = L$ if cells are placed side by side and $d = \sqrt{2}L$ if cells are placed along the diagonal. The slope factor is calculated according to Eq. 4, where a is a positive constant so that uphill fire spread is enhanced. By optimisation, $a = 0.078$ [7].

$$\theta_s = \tan^{-1}\left(\frac{H_1 - H_2}{d}\right) \tag{3}$$

$$p_s = \exp\left(a\theta_s\right) \tag{4}$$

The number and type of vegetation categories can be as refined as one wishes as long as the values attributed to each category reflect how flammable each category is. We opted to distinguish between only two types of vegetation, (i) forests and shrubs and (ii) agriculture, since we assume that shrubs are not less flammable than forests. The values we employ in our model are indicated in Table I.

TABLE I: Values of p_{veg} attributed to each considered type of land cover: forests, shrubs, agricultural land, rivers and roads.

Type of cover	p_{veg}
Forests & shrubs	0.4
Agriculture	-0.3
Rivers	-0.7
Roads	$[-0.6, -0.4]$

B. Modified model

Freire *et al.* introduced an extra rule to the Alexandridis model of fire spread and applied the modified model to simulate the wildfire that occurred in Tavira, in 2012 [9]. According to this rule, fire can propagate from a single source cell to n cells placed along the wind direction when wind speed is greater than a certain threshold.

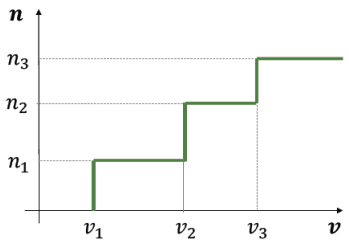

FIG. 2: Number of burned cells along the wind direction, n, as a function of wind speed, v. The applied wind rule can be represented as a step function where different wind speed thresholds, v_1, v_2 and v_3, provide different number of cells to be burned at a single time step, n_1, n_2 and n_3.

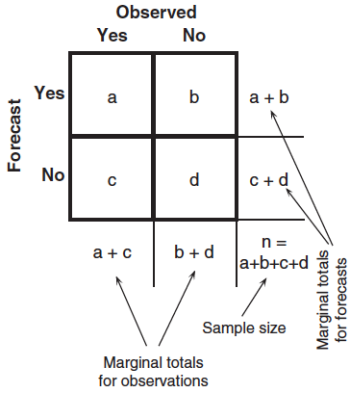

FIG. 3: Data organized in a contingency table. Columns contain data of what it is considered to be the truth against which one wants to validate the results obtained by the forecast (rows). Adapted from Wilks [18]

The number of cells to be burned is determined by a step function, such as the function represented in Fig. 2.

In our model, we included this wind rule, but we changed the way it is applied. On the one hand, only cells whose p_{veg} value is greater than -0.3 can be ignited. On the other hand, fire is allowed to jump over cells which cannot be ignited. With this rule, we can thus mimic the effect of spotting and promote fire propagation along the fire direction.

C. Verification and Validation of the models

We made use of contingency tables to assess the level of agreement of simulations' results with the reference data [18]. Fig. 3 shows a contingency table and the meaning of each one of its entries. In our case, "yes" means burned and "no" not burned. Each entry contains the number of cells that burned both in the reference and in simulation, a, not in the reference but in the simulation, b, in the reference and not in the simulation, c, and not burned in either, d. However, since we performed an ensemble of simulations, such hard classification is not appropriate. We thus resorted to fuzzy classification which allows for partial agreement to be considered [19]. We had as output data of our simulations a matrix whose entries contained relative burning frequencies for each cell, f. The values of f indicate partial agreement with observation if the corresponding cell burned in reference. Otherwise, partial agreement is given by $1 - f$ (not burned in reference, not burned in the ensemble). The fuzzy contingency table is then filled according to the following expressions:

$$\begin{cases} a' = \sum_{i,j}^{n,m} R_{ij} s_{ij} \\ b' = \sum_{i,j}^{n,m} \left(1 - R_{ij}\right) s_{ij} \\ c' = \sum_{i,j}^{n,m} R_{ij} \left(1 - s_{ij}\right) \\ d' = \sum_{i,j}^{n,m} \left(1 - R_{ij}\right)\left(1 - s_{ij}\right) \end{cases} \tag{5}$$

where Rij are the entries of the real burned area matrix ($R_{ij} = 1$ if (i, j) burned in reality, $R_{ij} = 0$ otherwise), s_{ij} contains the relative burning frequency of cell (i, j) in the simulation ensemble, n and m are the number of rows and columns, respectively.

Several indices can be computed from the entries of contingency tables, such as, overall agreement (OA), Dice index (DC), commission (CE) and omission (OE) errors and bias (B). These are a measure of agreement, reliability or bias of the forecasts:

$$OA = \frac{a + d}{n} \tag{6}$$

$$DC = \frac{2a}{2a + b + c} \tag{7}$$

$$CE = \frac{b}{n} \tag{8}$$

$$OE = \frac{c}{n} \tag{9}$$

$$B = \frac{a + b}{a + c} \tag{10}$$

For example, Dice index express agreement of forecasts with observations. The former is defined as the ratio between the sum of the diagonal entries and the total number of cells (Eq. 6). Dice index differs from OA in emphasising the "yes"-"yes" counts and ignoring the "no"-"no" counts, as is expressed by Eq. 7 [18]. CE index measures the relative counts of false positives (Eq. 8), whereas OE index quantify the relative number of false negatives in the forecasts (Eq. 9) [20]. The last index we consider here is the bias index. This index is the ratio between the "yes" forecast counts and the "yes" observation counts, as shown in Eq. 10. Unbiased results correspond to $B = 1$. This index makes no mention of agreement between forecasts and observations [20].

D. Input data

The elevation data required to calculate slopes of neighbouring cells were provided by SRTM (Shuttle Radar Topography Mission) digital elevation model [21].

Wind speed and direction matrices were updated for every elapsed hour of the simulations. These data resulted from running the regional model WRF (Weather

Research Forecast, version 4.0) [22]. Then, wind data were corrected for the topographic effect by WindNinja (version 3.4.1) [23].

Vegetation and initial state matrices were obtained from classifying land cover with 100 m resolution raster maps provided by CORINE data set (Coordination of information on the environment, CLC2012) [24].

Our main source of how wildfires evolved over time is the report done by a multidisciplinary team as a request of the Portuguese Parliament [3]. There, we find maps where hourly fire perimeters are indicated by isochrones. We complemented this information with satellite data, in particular, data provided by MODIS and VIIRS products of active fire detection: MCD14DL (collection 6, 1 km resolution) [25], and VNP14IMGTDL_NRT (375 m resolution) [26], respectively.

Almost all burned area shapefile maps were obtained from EFFIS (European Forest Fire Information System) [27]. The exception was Quiaios (Figueira da Foz). To obtain a map of Quiaios' burned area with the same level of detail as the reference map, we performed its mapping ourselves using Sentinel-2 of burned areas and followed the methodology described in Rus-Copernicus tutorial [28].

We resorted to ICNF's (Instituto da Conservação da Natureza e das Florestas) [29] burned area shapefiles to gather information on where and when the different fire events started and ended. This information was confirmed and complemented with the information presented by the report on the October fire events [3].

IV. CASE STUDIES

During the October wildfire episode (15-17 October) a total of 223,901 ha burned. On October 15, meteorological conditions were set for extreme fire behaviour to occur [30]: temperatures of 30°C, relative humidity lower than 30%, dead fuel moisture content between 3% and 6%, and last but not least, strong winds. Average wind speed reached values of 30-40 km/h and maximum wind speeds were as high as 50-80 km/h. The wind was strongest in central Portugal, where most of the wildfires took place. Direction of fire propagation was determined by wind direction: from south to north. These fires were wind-driven, although pyroconvection played an important role in the development of these fire events [3]. Pyroconvection designates phenomena that arise from the interaction of fire with atmosphere, locally changing the weather. Fireline intensity, energy emitted per unit time and unit length by an active fire [30], associated with the observed fire propagation speeds was estimated to be too high for suppression efforts to have had effect. Therefore, these fires progressed mostly unconstrained, where wind-induced spotting was responsible for generating new ignitions at distances as great as 500-2000 m from the fire perimeter [3].

We implemented the already mentioned CA fire spread models to simulate four of the large fire events that took place on October 15: Pataias-Burinhosa, Quiaios (Figueira da Foz), Sertã and Arganil. Fig. 4 shows the geographical location of the case studies.

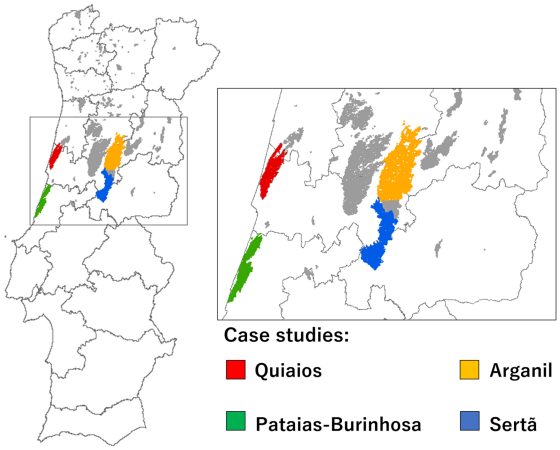

FIG. 4: Map of Portugal with the location of the case studies: Pataias-Burinhosa, Quiaios (Figueira da Foz), Sertã and Arganil. The remaining area burned on 15-17 October is represented in grey.

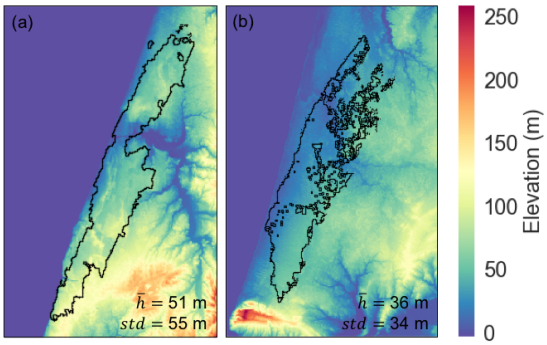

FIG. 5: Elevation profiles of the regions where coastal wildfires took place: (a) Pataias-Burinhosa; (b) Quiaios (Figueira da Foz). Black lines represent the real fire perimeters. Elevation values in these regions range between 0 m and 250 m, showing average elevations, $\bar{h}$, of (a) 51 m and (b) 36 m. Standard deviations, *std*, are (a) 55 m and (b) 34 m.

Wildfires that took place near the coast developed similarly, but differently from the fires that occurred in inland regions. Both coastal wildfires, Pataias-Burinhosa and Quiaios, show an elongated shape, which reflects the influence of the wind in their development. It is also noteworthy that, in all cases, fire consumed most of the total burned area by the end of the first day, although these fires were only fully under control around the end of October 16 or during the first hour of October 17. The linear progress of these wildfires can be attributed to the characteristics of the terrain: fairly flat and homogeneous land cover [3]. Fig. 5 shows that these regions have low values of elevation (average elevations values of the study areas for Pataias-Burinhosa and Quiaios are 51 m and 36 m, respectively), with small variability (standard deviation values are 55 m (Pataias-Burinhosa) and 34 m (Quiaios)). The land cover maps in Fig. 6 were obtained from classifying CLC2012 codes [24] into four categories: non-flammable, agriculture, shrubs, forests. These show that the land enclosed by the fire perimeter was covered by mostly forest and patches of shrubs.

The regions where Sertã's and Arganil's wildfires took

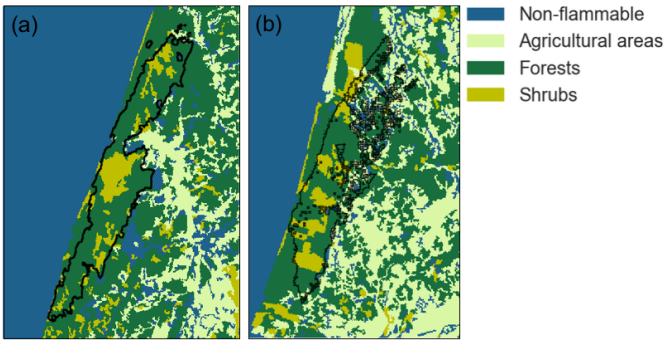

FIG. 6: Coastal regions' land cover maps obtained from CLC2012 [24], where fire perimeters are indicated in black: (a) Pataias-Burinhosa; (b) Quiaios (Figueira da Foz). CLC2012 information was classified into four categories: non-flammable, agricultural areas, forests and shrubs. These maps show that the coastal burned areas used to be covered by forests and shrubs.

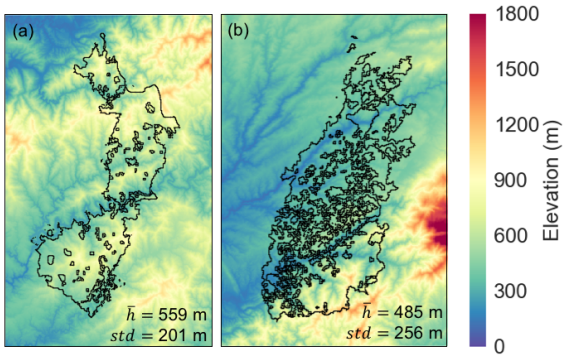

FIG. 7: As in Fig. 5, but for elevation maps of inland study areas: (a) Sertã; (b) Arganil. Elevation colorbar shows values within a wider interval, 0-1800m, than in Fig. 5. Average values of elevation, $\bar{h}$, are (a) 559 m and (b) 485 m. Standard deviations of elevation were found to be (a) 201 m and (b) 256 m.

place show heterogeneous topographic profiles (Fig. 7) and discontinuous land cover (Fig. 8). Such terrain's features combined with pyroconvection resulted in a more complex development of these fires, in comparison with the coastal wildfires [3]. Elevation profiles of the study areas have average elevations equal to 559 m (Sertã) and 485 m (Arganil), presenting much greater standard deviations values than the ones calculated for the coastal regions (201 m (Sertã) and 256 m (Arganil)). The areas delimited by the fire perimeters have discontinuous and heterogeneous land cover, being Arganil the region with the most fragmented cover.

In Table II, we included the values of the area burned in each case study, as well as the time required for fire to be controlled. The dimensions of our study areas (length and width) are also shown.

Pataias-Burinhosa's wildfire started with an ignition in Pataias at 2:01 pm, followed by a second ignition at 2:33 pm, in Burinhosa (northeast from the first ignition). Most of its 16,949.6 ha burned on the first day. This fire event was only contained on October 17 at 00:37 after two hours of rainfall.

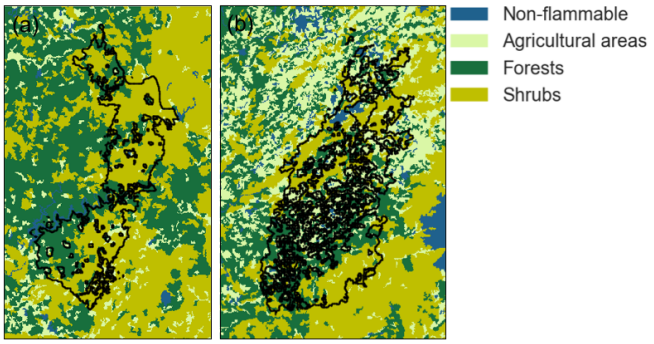

FIG. 8: As in Fig. 6, but for land cover of inland case studies: (a) Sertã; (b) Arganil. Land cover is less homogeneous and continuous than in the case of the coastal regions. In particular, the area of Arganil where the wildfire occurred had a quite heterogeneous cover with agricultural fields surrounded by forests and shrubs.

TABLE II: Dimensions of study area for each case study (length, l, and width, w), corresponding total burned area, BA, and duration of fire events [3].

Case study	l(km)	w(km)	BA(ha)	Duration(h)
Pataias	47.1	33.4	16,949.6	34.6
Quiaios	42.6	27.0	19,025.5	32.7
Sertã	51.5	32.0	33,192.6	38.0
Arganil	57.6	39.1	38,811.0	41.1

Quiaios' wildfire originated from a single ignition located at the most southern point of its fire perimeter. It was first reported at 2:36 pm. This wildfire was dominated at 11:16 pm on the following day. During that period, an area of 19,025.5 ha was consumed by fire. Fire spread fastest between 4:00 and 8:00 pm of the first day of burning, with an average value of 4.8 km/h and reaching up to 5.4 km/h [3].

Sertã's fire had its start at 12:02 pm, in Figueiredo. Six and a half hours later, a second ignition took place in Pedrogão Novo. The location of the latter prevented it from having an important contribution to the way Sertã's wildfire developed, since the growth of this ignition was constrained by the burned area of Pedrogão Grande (burned in June 2017) in the west and north and, in the east, by the active fire that started in Figueiredo.

Some ember carried by the wind traversed Cabril dam and gave rise to a new fire in Machio (8:00 pm). From this point, fire propagated fast, reaching the average speed of 6 km/h. Propagation only considerably slowed down after 3:00 am of the following day. Fire was controlled at 2:03 am on October 17.

The burned area of Pedrogão Grande, located west from Sertã's wildfire, acted as a barrier in the development of this fire event. It is believed that Sertã's wildfire would have reached much greater proportions if Pedrogão Grande's wildfire had not taken place [3].

Arganil's burned area was the result of four ignitions. The map containing information on its time evolution is less clear and the reference map obtained from it contains only a few reference time lines than the previous ones. The reference map was obtained from combining

the information in the report [3] with MODIS and VIIRS data. This wildfire is the second largest wildfire ever seen in the country, having burned 38,811 ha.

This wildfire started at 10:26 am, in Sandomil-Seia. The discontinuous vegetation cover prevented it from spreading fast. Two more ignitions, located southwest from the starting point, took place at 12:28 pm. These ignitions were only separated by 4 km: Relva Velha (east) and Monte Redondo (west). The last ignition took place at 11:00 pm in Seia (southeast region of the burned area). The wildfire was contained on October 17 at 03:32 am.

Of the four case studies, this fire event registered the highest growth rate, 6,968 ha/h, between 12:00 am and 1:00 am on October 16 [3].

V. RESULTS

We started by simulating the case studies' wildfires with the baseline model. We selected time steps $\Delta t =$ 2 min and $\Delta t = 3$ min for simulating wildfires that occurred in coastal and inland regions, respectively. These values were found through an estimate of the time required for a square cell of side $L = 100$ m to be burned, as obtained by dividing the linear distance advanced by fire by the time it took to reach that distance. The difference in time step between the two regions can be attributed to their difference in topography: coastal regions present flat terrain while inland regions show great variation in elevation.

The maps used as reference for progress of fire over time are shown in Fig. 9. Root-mean-square deviation (RMSD) and average deviation, i.e., temporal bias, are the quantities used to assess the level of spatiotemporal agreement. Fig. 10 shows the simulated time evolution (50th percentile) yielded by simulations performed with the baseline model. The spatiotemporal agreement is best for coastal wildfires, yielding RMSD of less than 2 h. However, their parallel isochrones come about as unrealistic and do not resemble the reference lines. The agreement of simulations of inland wildfires with the reference is much worse. Arganil's wildfire shows RMSD of more than 9 h and Sertã's simulated fire shows very poor spatial agreement.

To improve isochrones' shape of the coastal fires and spatial agreement of inland wildfires, in particular, Sertã' wildfire, we performed new simulations employing the modified model. The baseline time steps were found to be inadequate to simulate fire spread with the modified model, because the modified model accelerates fire propagation by allowing more than one cell to be set on fire from a single fire source. We arrived at $\Delta t_{modified} = 2\Delta t_{baseline}$.

Fig. 11 presents the 50th percentile time evolution maps of wildfires simulated with the baseline model. There is a clear improvement in the shape of isochronic lines in the case of coastal wildfires. These are now elongated and point towards the dominant direction of fire propagation. However, their overall spatiotemporal agreement slightly decreased as shown by the small increase of RMSD and bias values. The modified model yielded major improvements in spatial distribution of burned area in the case of Sertã. The reason of such

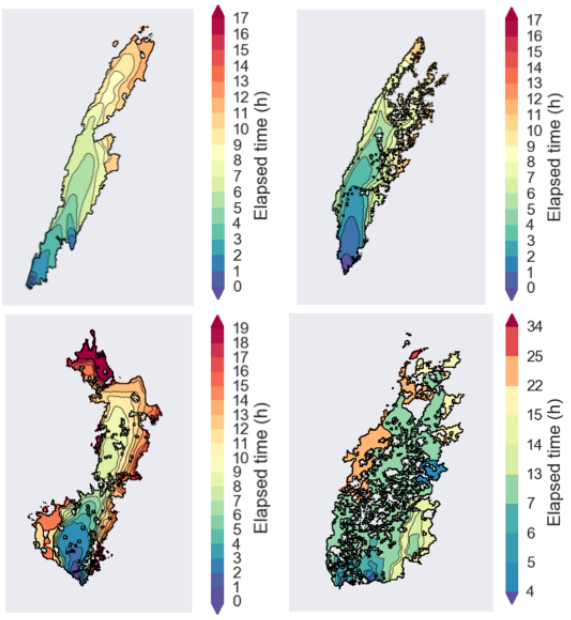

FIG. 9: Reference maps showing how fire evolved over time. Top, left to right: Pataias-Burinhosa and Quiaios. Bottom, left to right: Sertã and Arganil.

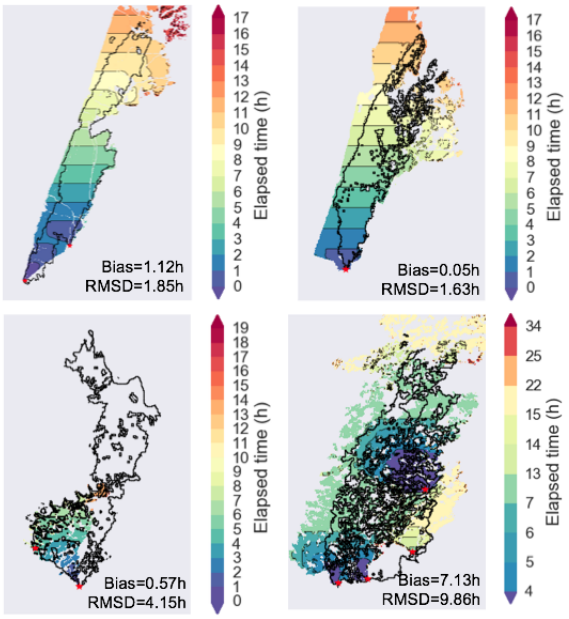

FIG. 10: 50th percentile maps showing progress of fire simulated with the baseline model (coastal wildfires: $\Delta t = 2$ min; inland wildfires $\Delta t = 3$ min). Top, left to right: Pataias-Burinhosa and Quiaios. Bottom, left to right: Sertã and Arganil. Ignitions points are indicated by red starts. Values of RMSD and bias were calculated using the reference maps in Figure 9.

difference lies in the spotting effect being captured by the wind rule included in the modified model. This tells us that Sertã's fire spread mostly occurred by means of embers carried by the wind, surpassing obstacles and generating new ignitions in isolated locations. The modified model did not simulate the effect of the second reported ignition, because the region where it occurred was burned in the first three hours of simulation. However, we still

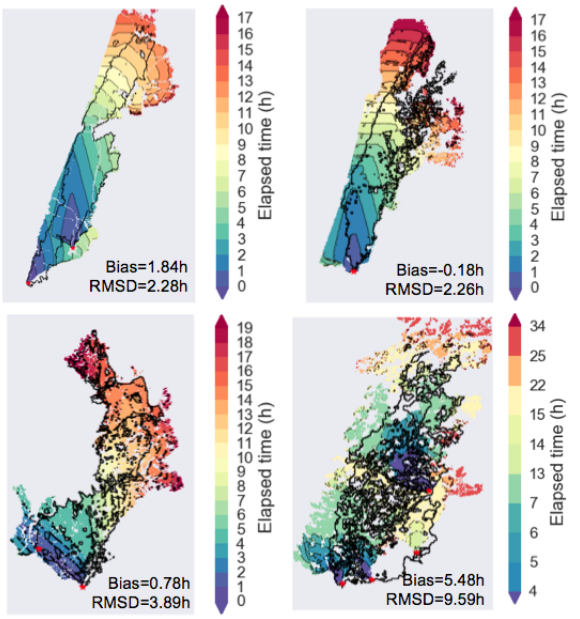

FIG. 11: As in Fig. 10, but simulations performed with the modified model (time steps $\Delta t = 4$ min and $\Delta t = 6$ min for coastal and inland wildfires, respectively).

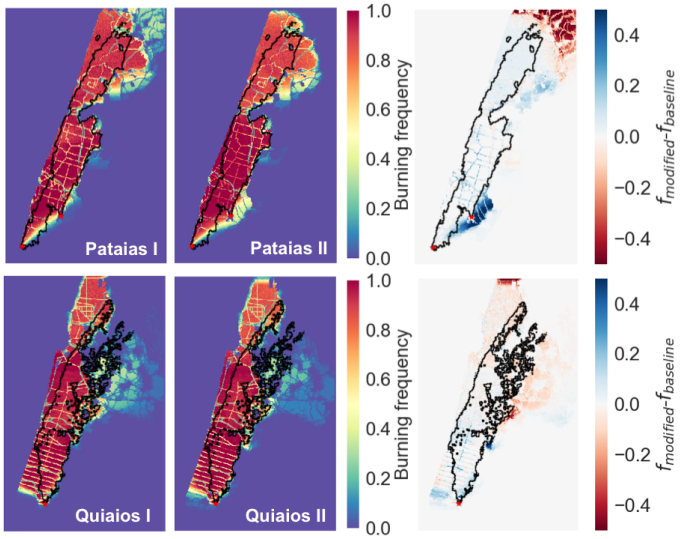

FIG. 12: Maps of burning frequencies obtained for the simulations of the coastal wildfires, applying (I) the baseline (left) and (II) the modified models (middle). The map on the right was obtained from taking the difference between the first two maps. Blue (red) regions indicate higher burning frequency values for simulations performed with baseline (modified) model. Top: Pataias-Burinhosa; bottom: Quiaios (Figueira da Foz).

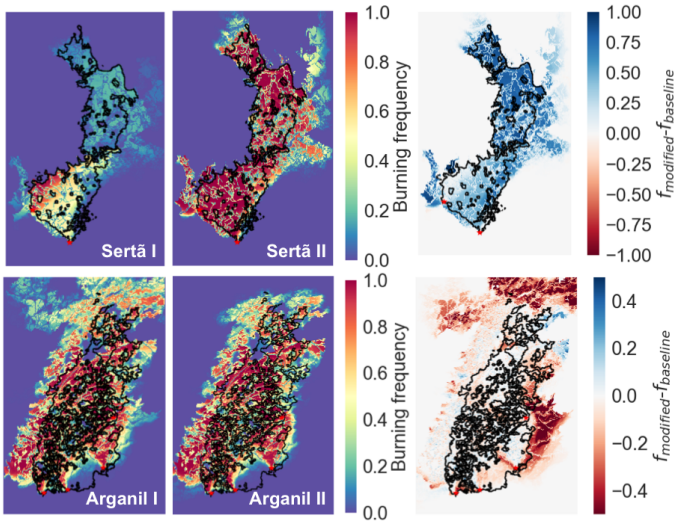

FIG. 13: As in Fig.12, but now showing distribution of burning frequencies for the wildfires that occurred in inland regions: Sertã (top) and Arganil (bottom).

obtained good agreement with the reference, which confirms that this ignition did not crucially affect fire propagation, as stated in report [3].

Simulations of Arganil's wildfire performed with the modified model did not produce substantial improvements. RMSD value was found to be still over 9 h and spatial distribution of burned area slightly improved.

Fig. 12 and Fig. 13 present how the relative burning frequencies obtained from employing the baseline and the modified models distribute and how they compare (difference map) for the coastal and inland wildfires, respectively. Except for Sertã's wildfire, the spatial distributions of burning frequencies shown for both models are very similar. That was to be expected, since these models have most rules in common and thus respond similarly to the underlying land cover. Fig. 14 shows that high frequency values ($f > 0.5$) are associated with flammable types of land cover. That is the case for all the simulations except when employing the baseline model to simulate Sertã's wildfire. Therefore, Fig. 14 only refers to simulations performed with the modified model.

Simulations of Sertã's wildfire performed with the modified model have Dice value equal to 0.7. This value confirms the improvement produced by the introduction of the wind rule, since the baseline model yielded small values of Dice and bias indices ($DC = 0.4$ and $B = 0.4$) and large omission error ($OE_{baseline} = 0.14$ vs. $OE_{modified} = 0.06$). Simulations of Pataias-Burinhosa's (both models) and Sertã's (modified) wildfires present the best spatial agreement ($DC = 0.7$). These are then followed by Quiaios' simulations ($DC = 0.6$). Arganil's simulated wildfire has Dice values of 0.5 (baseline) and 0.6 (modified).

We performed further simulations of Sertã's wildfire, but without taking into account the surrounding area burned in the wildfires that occurred earlier that year. Fig. 15 presents distribution of fire for three different values of elapsed time and highlights the fire perimeter of Pedrogão Grande (June 2017). This shows that this area would have a high chance of burning in October 2017 if it had not burned before. This result agrees with what is shown in report [3].

To determine the viability of these CA fire spread models as operational tools, we studied how burning frequencies of cells' inside and outside the real fire perimeter compare. Fig. 16 shows the proportions of high ($f > 0.5$) and low ($f \leq 0.5$) relative burning frequencies for cells inside and outside the fire perimeter. These histograms refer to simulations performed with the modified model, since the other model yields analogous results (except

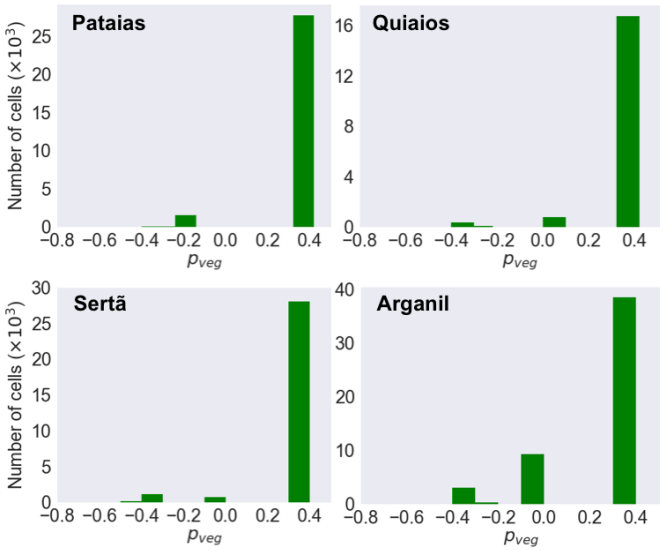

FIG. 14: Histograms of p_{veg} values for cells that burned in more than 50% of simulations ($f > 0.5$) performed with the modified model. Top row refers to coastal wildfires: Pataias-Burinhosa (left) and Quiaios (right). Bottom row: Sertã (left) and Arganil (right).

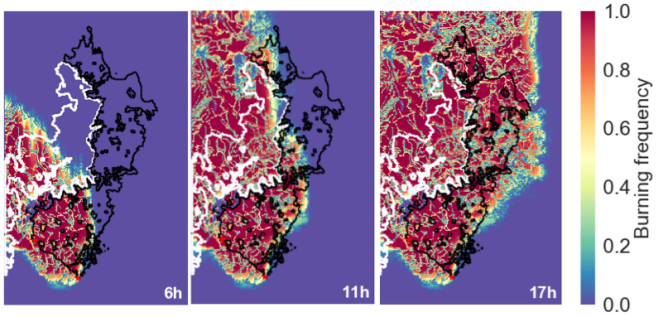

FIG. 15: Burning frequency maps obtained from simulating Sertã's wildfire without taking into account areas that burned earlier that year. Each map shows simulations' results for different values of elapsed time, from left to right: 6 h, 11 h, 17 h. The black line indicates the real burned perimeter of Sertã. The white line represents the fire perimeter of the large fire event that took place in Pedrogão Grande in June 2017.

.

for Sertã's wildfire). In general, most cells inside the fire perimeter were found to have high frequency values, whereas cells outside tended to burn less frequently. The box plots in Fig. 17 confirm this trend. Furthermore, these show that the upper quartile of burning frequencies outside is greater than 0.8 in the case of Pataias-Burinhosa, and is always less than that for all the other case studies. Burning frequencies inside have upper quartiles greater than 0.8. This result allowed us to choose 0.8 as a burning frequency threshold above which most real burned area is represented and only a small proportion of burned area outside the fire perimeter is visible, as shown in Fig. 18.

The operational potential of CA fire spread models lies in their capacity to determine accurately regions of high and low fire risk to assist in fire combat management. Fire suppression resources must be placed in low fire risk

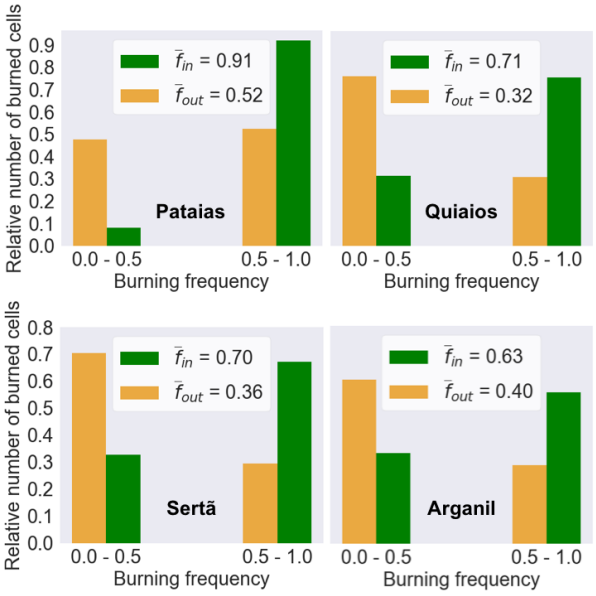

FIG. 16: Histograms of burning frequencies showing the relative counts of cells burning outside (orange) and inside (green) the area burned in reality. Only the results of simulations employing the modified model are shown. The legends contain the average burning frequencies for both cells inside ($\bar{f}_{in}$) and outside the real fire perimeter ($\bar{f}_{out}$). We further indicate the number of burned cells inside, n_{in}, and outside, n_{out}. Top, coastal wildfires: Pataias-Burinhosa (left), with $n_{in} = 19,813$ and $n_{out} = 21,495$, and Quiaios (right), with $n_{in} = 15,631$ and $n_{out} = 23,973$. Bottom, inland wildfires: Sertã (left), with $n_{in} = 30,649$ and $n_{out} = 32,458$, and Arganil (right), with $n_{in} = 49,847$ and $n_{out} = 64,044$.

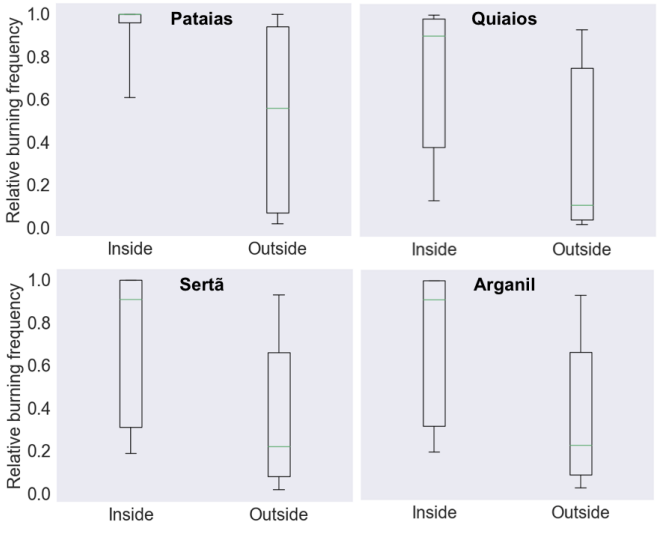

FIG. 17: Box plots of relative burning frequencies of cells inside and outside the real fire perimeter obtained from 100-simulation ensemble performed with the modified model. Upper (lower) whisker extends to the 90th (10th) percentile of the data. Top box plots were obtained from the coastal wildfires: Pataias-Burinhosa (left) and Quiaios (right). Bottom: inland fires (Sertã, on the left, and Arganil, on the right).

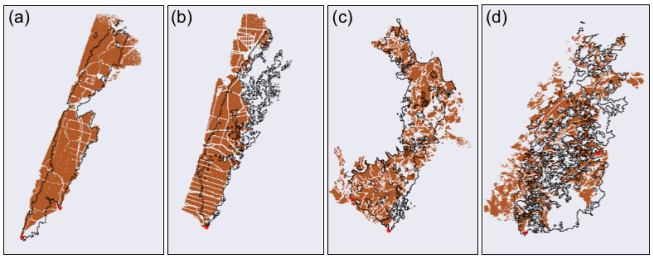

FIG. 18: Maps showing 80th percentile simulated burned area obtained from 100-simulation ensemble: (a) Pataias-Burinhosa, (b) Quiaios, (c) Sertã and (d) Arganil. For the burning frequency threshold of 0.8, most of burned cells lie inside fire perimeter. Cells outside are, therefore, less likely to burn.

regions in the neighbourhood of the active fire. CA fire spread models can thus help in managing resources in a more efficient and safer way.

VI. CONCLUSIONS

Our work shows that the employed CA models of fire spread are suitable to simulate fire propagation. A modified model was obtained from the baseline model by introducing a wind rule that allows for fire to be spread to a number of cells placed along the wind direction, when wind speed is high enough. It further mimics spotting effect by allowing fire to jump over cells.

In the case of coastal wildfires, the modified model yielded isochrones whose shape is reasonably close to the shape of time lines. In the case of Sertã's wildfire, the modified model outperformed the baseline model regarding spatial distribution of burned cells, which confirms that spotting was instrumental in the spread of fire in this region. In the end, Sertã's simulated fire shows good spatial agreement with the real wildfire (Dice value of 0.7).

Simulations of coastal wildfires show the best spatiotemporal agreement with the reference maps (RMSD of about 2 h for both models). Their spatial distributions of relative burning frequencies also agree fairly well with the references (Dice values of 0.7 and 0.6 for Pataias-Burinhosa's and Quiaios' wildfires, respectively).

In both temporal and spatial aspects, both models performed the worst when simulating Arganil's wildfire. The modified model yielded slight improvements, but still showing poorer agreement with reality than the previous cases. Heterogeneous landscape, interaction of four ignitions and lack of detailed information on fire progress can partly explain these results. In addition, it is known that pyroconvection played a role in the development of this fire and our models cannot simulate the occurrence of this phenomenon.

We tested the effect of the occurrence of earlier wildfires on fire spread in Sertã. Simulations performed without taking into account area burned by those fires shows that Sertã's fire progress was very constrained and regions like Pedrogão Grande could have been burned in October 2017 if these had not burned before.

Our results further demonstrate that these CA fire spread models can play a role in fire combat. The CA fire spread models identified the regions enclosed by the real fire perimeter as having high risk of burning ($f > 0.5$) and regions outside as having lower risk ($f \leq 0.5$). This shows that CA fire spread models can determine which locations are safe and effective to place fire suppression resources. Extra rules can also be added to simulate the effect of human intervention on fire spread.

[1] Incêndios florestais e área ardida. URL `https://www.pordata.pt/Europa/Incndios+florestais+e+rea+ardida-1374`. Last access: 26-02-2019.

[2] I. Departamento de Gestão de Áreas Públicas e de Proteção Florestal. Relatório provisório de incêncios florestais 2017: 01 de Janeiro a 31 de Outubro. Technical report, ICNF, 2017. URL `http://www2.icnf.pt/portal/florestas/dfci/Resource/doc/rel/2017/10-rel-prov-1jan-31out-2017.pdf`. Last access: 04-03-2019.

[3] J. G. Comissão Técnica Independente, C. Fonseca, A. Salgueiro, P. Fernandes, E. L. Iglésias, R. de Neufville R., F. Mateus, M. Castellnou, J. Silva, J. Moura, F. Rego, and D. C. Coords. Avaliação dos incêndios ocorridos entre 14 e 16 de outubro de 2017 em Portugal Continental. Relatório Final. Comissão Técnica Independente. Technical report, Assembleia da República, 2018. URL `https://www.parlamento.pt/Documents/2018/Marco/RelatorioCTI190318N.pdf`. Last access: 04-03-2019.

[4] Y. Liu, J. Stanturf, and S. Goodrick. Trends in global wildfire potential in a changing climate. *Forest Ecology and Management journal*, 259:685–697, 2010. doi: 10.1016/j.foreco.2009.09.002.

[5] M. Pereira, T. Calado, C. DaCamara, and T. Calheiros. Effects of regional climate change on rural fires in Portugal. *Climate Research*, 57:187–200, 2013. doi: 10.3354/cr01176.

[6] R. Rothermel. A mathematical model for predicting fire spread in wildland fuels. *USDA Forest Service, Intermountain Forest and Range Experiment Station*, 1972.

[7] A. Alexandridis, D. Vakalis, C. Siettos, and G. Bafas. A cellular automata model for forest fire spread prediction: The case of the wildfire that swept through Spetses Island in 1990. *Applied Mathematics and Computation*, 204(1): 191 – 201, 2008. doi: 10.1016/j.amc.2008.06.046.

[8] A. Alexandridis, , L. Russo, D. Vakalis, G. Bafas, and C. Siettos. Wildland fire spread modelling using cellular automata: Evolution in large-scale spatially heterogeneous environments under fire suppression tactics. *International Journal of Wildland Fire*, 20(5):633–647, 2011. doi: 10.1071/WF09119.

[9] J. Freire and C. DaCamara. Using cellular automata to simulate wildfire propagation and to assist in fire management. *Nat. Hazards Earth Syst. Sci.*, 19:169–179, 2019. doi: 10.5194/nhess-19-169-2019.

[10] S. Wolfram. *A New Kind of Science*. Wolfram Media Inc, 1st edition edition, 2002. ISBN 1-57955-008-8.

[11] I. Karafyllidis and A. Thanailakis. A model for pre-

dicting forest fire spreading using cellular automata. *Ecological Modelling*, 99(1):87–97, 1997. doi: 10.1016/S0304-3800(96)01942-4.

[12] X. Li and W. Magill. Modeling fire spread under environmental influence using a cellular automaton approach. *Complexity International*, 8:1–14, 2001. URL `https://pdfs.semanticscholar.org/2bb3/842da1d924dc7ef20a0c8784e8b9be997c11.pdf`. Last access: 13-05-2019.

[13] G. Trunfio. Predicting Wildfire Spreading Through a Hexagonal Cellular Automata Model. *Lecture Notes in Computer Science: Cellular Automata, Proceedings*, 3305:385–394, 2004. doi: 10.1007/978-3-540-30479-1_40.

[14] J. Amorim, C. Borrego, and A. Miranda. Development and validation of an operational numerical model for the simulation of the aerial drop of firefighting products. In *Eighth Symposium on Fire and Forest Meteoreology*. American Meteorological Society, 2009. URL `http://ams.confex.com/ams/pdfpapers/156292.pdf`. Last access: 04-03-2019.

[15] M. Avolio, W. Spataro, S. D. Gregorio, and G. Trunfio. Wildfire Hazard Mapping Using Cellular Automata. *International Conference on Scientific Computing (CSC 2011)*, pages 191–197, 2011. URL `http://cerc.wvu.edu/download/WORLDCOMP'11/2011CDpapers/CSC5195.pdf`. Last access: 05-03-2019.

[16] L. Russo, P. Russo, and C. Siettos. Reducing Wildland Fire Hazard Exploiting Complex Network Theory: a Case Study Analysis. *Chemical Engineering Transactions*, 53:19–24, 2016. doi: 10.3303/CET1653004.

[17] A. Ohgai, Y. Gohnai, S. Ikaruga, M. Murakami, and K. Watanabe. Japan Cellular Automata Modeling for Fire Spreading as a Tool to Aid Community-Based Planning for Disaster Mitigation. *Recent Advances in Design & Decision Support Systems in Architecture and Urban Planning*, pages 193–209, 2004. doi: 10.13140/2.1.4752.8001.

[18] D. S. Wilks. *Statistical Methods in the Atmospheric Sciences*, volume 91 of *International Geophysics Series*. Academic Press, 2nd edition, 2006. ISBN 0-12-751966-1.

[19] E. Binaghi, P. Brivio, G. P., and R. A. A fuzzy set-based accuracy assessment of soft classification. *Pattern Recognition Letters*, 20:935–948, 1999. doi: https://doi.org/10.1016/S0167-8655(99)00061-6.

[20] R. Libonati, C. C. D. Camara, A. W. Setzer, F. Morelli, and A. E. Melchiori. An Algorithm for Burned Area Detection in the Brazilian Cerrado Using 4 μm MODIS Imagery. *Remote Sensing*, 7:15782–15803, 2015. doi: 10.3390/rs71115782.

[21] T. G. Farr, P. A. Rosen, E. Caro, R. Crippen, R. Duren, S. Hensley, M. Kobrick, M. Paller, E. Rodriguez, L. Roth, D. Seal, S. Shaffer, J. Shimada, J. Umland, M. Werner, M. Oskin, D. Burbank, and D. Alsdorf. The Shuttle Radar Topography Mission. *Reviews of Geophysics*, 45(RG2004), 2007. doi: https://doi.org/10.1029/2005RG000183.

[22] W. Skamarock, J. B. Klemp, J. Dudhia, D. O. Gill, Z. Liu, J. Berner, W. Wang, J. G. Powers, M. G. Duda, D. M. Barker, and X.-Y. Huang. *A Description of the Advanced Research WRF Version 4. NCAR Tech. Note NCAR/TN-556+STR*, 2019. doi: 10.5065/1dfh-6p97.

[23] J. M. Forthofer, B. W. Butler, and N. S. Wagenbrenner. A comparison of three approaches for simulating fine-scale surface winds in support of wildland fire management. Part I. Model formulation and comparison against measurements. *Int. J. Wildland Fire*, 23(7):969–981, 2014. doi: https://doi.org/10.1071/WF12089.

[24] CLC2012: The CORINE Land Cover (CLC) dataset produced in 2012. URL `https://land.copernicus.eu/pan-european/corine-land-cover/clc-2012?tab=download`. Last access: 09-03-2019.

[25] NASA Near Real-Time and MCD14DL MODIS Active Fire Detections (SHP format). Data set. URL `https://earthdata.nasa.gov/active-fire-data`. Last access: 30-04-2019.

[26] NASA Near Real-Time VNP14IMGTDL_NRT VIIRS 375 m Active Fire Detections (SHP format). Data set. URL `https://earthdata.nasa.gov/active-fire-data`. Last access: 30-04-2019.

[27] J. San-Miguel-Ayanz, E. Schulte, G. Schmuck, A. Camia, P. Strobl, G. Libertà, C. Giovando, R. Boca, F. Sedano, P. Kempeneers, D. McInerney, C. Withmore, S. Santos de Oliveira, M. Rodrigues, T. Durrant, P. Corti, F. Oehler, V. L., and G. Amatulli. Comprehensive monitoring of wildfires in Europe: the European Forest Fire Information System (EFFIS). In J. Tiefenbacher, editor, *Approaches to Managing Disaster - Assessing Hazards, Emergencies and Disaster Impacts*. InTech, 2012. ISBN 978-953-51-0294-6.

[28] Training kit - HAZAO2: Burned area mapping with Sentinel-2 using SNAP June, Portugal. URL `https://rus-copernicus.eu/portal/wp-content/uploads/library/education/training/HAZA02_BurnedArea_Portugal_Tutorial.pdf`. Last access: 09-03-2019.

[29] Mapas de áreas ardidas ICNF. URL `http://www2.icnf.pt/portal/florestas/dfci/inc/mapas`. Last access: 30-04-2019.

[30] D. X. Viegas. Extreme Fire Behaviour. In A. Bonilla Cruz and R. Guzman Correa, editors, *Forest Management: Technology, Practices and Impact*. Nova Science Publishers, 2012. ISBN 978-1620813591.